https://doi.org/10.5194/acp-2020-1010
Preprint. Discussion started: 27 October 2020

Atmospheric Chemistry and Physics Discussions

Processes influencing lower stratospheric water vapour in monsoon anticyclones: insights from Lagrangian modeling

Nuria Pilar Plaza[1], Aurélien Podglajen[2], Cristina Peña-Ortiz[1], and Felix Ploeger[3,4]

[1]Área de Física de la Tierra. Departamento de Sistemas Físicos, Químicos y Naturales. Universidad Pablo de Olavide, Sevilla, Spain
[2]Laboratoire de Météorologie Dynamique (LMD/IPSL), École polytechnique, Institut polytechnique de Paris, Sorbonne Université, École normale supérieure, PSL Research University, CNRS, Paris, France
[3]Institute of Climate Research. Forschungszentrum Jülich, Jülich, Germany
[4]Institute for Atmospheric and Environmental Research, University of Wuppertal, Wuppertal, Germany

Correspondence: Nuria Pilar Plaza (npplamar@upo.es)

Abstract. We investigate the influence of different chemical and physical processes on the water vapour distribution in the lower stratosphere (LS), in particular in the Asian and North-American monsoon anticyclones (AMA and NAMA, respectively). Specifically, we analyze effects of large-scale temperatures, methane oxidation, ice microphysics, and small-scale atmospheric mixing processes in model experiments with the chemistry transport model CLaMS. All these processes hydrate the LS, in particular over the Asian Monsoon. While ice microphysics has the largest global moistening impact, it is small-scale mixing which dominates the specific signature in the AMA. In particular, the small-scale mixing parameterization strongly contributes to the seasonal and intra-seasonal variability of water vapour in that region and including it in the model simulations results in a significantly improved agreement with observations. Although none of our experiments reproduces the spatial pattern of the NAMA seen in MLS observations, they all exhibit a realistic annual cycle and intra-seasonal variability, which are mainly controlled by temperatures. We further analyse the sensitivity of these results to the domain-filling trajectory set-up used in the five model experiments, here-called Lagrangian Trajectory Filling (LTF). Compared with MLS observations and with a multiyear reference simulation using the standard version of CLaMS, we find that LTF schemes result in a drier global LS and drier water vapour signal over the monsoon regions. Besides, the intra-seasonal variability of water vapour in the AMA is less correlated with MLS during June–August. We relate these results to the fact that the LTF schemes produce a low density of air parcels in the moistest areas of the AMA.

1 Introduction

Water vapour in the lower stratosphere (LS) is one of the most important chemical species because of its impact on the global radiative budget (Solomon et al., 2010; Riese et al., 2012). Its distribution in the upper troposphere-lower stratosphere (UTLS) depends on the strength of the Brewer–Dobson circulation, the quasi-horizontal isentropic transport between tropical and

https://doi.org/10.5194/acp-2020-1010
Preprint. Discussion started: 27 October 2020


Atmospheric Chemistry and Physics Discussions

high latitudes and the convective activity that enhances the cross-isentropic transport (Fueglistaler and Haynes, 2005; Diallo et al., 2018; Poshyvailo et al., 2018). The Brewer–Dobson circulation lifts up moist air from the troposphere into the deep stratosphere through the Tropical Tropopause Layer (TTL). In this layer, air masses encounter the coldest temperatures of the tropopause, the so-called Cold Point Tropopause (CPT) (Fueglistaler et al., 2005), and dehydrate. Thus, on different timescales, the variability of water vapour entering the stratosphere is closely related to the variability of CPT temperature (Fueglistaler and Haynes, 2005). An example of this relation is the tape recorder water vapour signal in the tropical stratosphere (Mote et al., 1996), which shows the upward propagation of water vapour anomalies to the seasonal cycle of the tropopause temperatures. However, the control of water vapour anomalies by the CPT weakens during boreal summer, when maxima of water vapour in the UTLS are found over the Asian and North American monsoon regions. This raises the question of the importance of the monsoon systems as a secondary pathway to transport water vapour into the LS.

Monsoon circulations appear as a dynamical response to diabatic heating released by persistent convection over regions close to the equator (Gill, 1980). In the case of the Asian Monsoon, convection has its climatological center over the Bay of Bengal, and generates the AMA, a strong planetary-scale anticyclone in the UTLS which is the most dominant feature in the global atmosphere during boreal summer (Hoskins and Rodwell, 1995). The rapid vertical transport in the inner core of the monsoon pumps up moist air masses from the troposphere directly into the UTLS. There, the strong anticyclonic winds of the monsoon circulation behave as a transport barrier (Ploeger et al., 2015) that isolate the air masses from outer regions, keeping the air with high water vapour content (and similar for other trace gases with tropospheric sources) confined (Randel and Park, 2006; Park et al., 2007; Randel et al., 2010; Santee et al., 2017). At this height, air masses slowly ascend through the cold tropopause, where they further dehydrate (Park et al., 2007). However, the mechanism of simple large-scale temperature control alone might not be sufficient to explain water vapour distributions by itself as air masses in the Asian monsoon UTLS are generally about 20–50% supersaturated (e.g., Krämer et al., 2020). In the case of the NAMA, there is less understanding of the water vapour signal observed, which is much stronger than for air under purely saturated conditions (Gettelman et al., 2004). However, as the anticyclonic circulation in the UTLS of the North American monsoon is much weaker, the sensitivity to processes also present in the Asian Monsoon, such as convection, is different (Dessler and Sherwood, 2004). Thus, besides tropical cold-point temperatures, multiple other factors influence the transport of water vapour to the LS.

The impact of convection has been the focus of several studies but remains controversial. While Dessler and Sherwood (2004); Dessler et al. (2007); Ueyama et al. (2018) and Gettelman et al. (2002a) found that convection, and especially overshooting events, increase the LS water vapour signal over the monsoon regions, other studies emphasized that the main role of convection is related to changes in diabatic heating rates and, hence, the dynamical structure of the region (Gettelman et al., 2002b; Park et al., 2007; Schoeberl et al., 2013; Randel et al., 2015; Zhang et al., 2016; Kim et al., 2018). Randel et al. (2015) found that stronger convection leads to relatively cold temperatures in the subtropical LS, which they identified as a key region controlling large-scale dehydration within the anticyclonic monsoonal circulation, giving rise to a drier stratosphere. Therefore, it is not clear whether the main role of convection is to moisten the LS through overshooting events or to dehydrate it by decreasing the tropopause temperatures.

https://doi.org/10.5194/acp-2020-1010
Preprint. Discussion started: 27 October 2020

Atmospheric Chemistry and Physics Discussions

Furthermore, Ueyama et al. (2018) concluded that in Lagrangian experiments convective processes are necessary to explain the water vapour signal over monsoon regions, while Schoeberl et al. (2013); Ploeger et al. (2013) and Poshyvailo et al. (2018) achieved realistic H2O distributions without any convective scheme. Thus, this apparent disagreement not only highlights the problem to understand the role of convection in LS water vapour simulations, but also the impact that the configuration of a model experiment might have on the LS water vapour distribution. Schoeberl et al. (2013) uses the model developed by Schoeberl and Dessler (2011) based on the domain-filling Lagrangian technique. This approach is based on the philosophy that LS water vapour depends on the processes acting in the upper troposphere and in the tropopause region and therefore assumes only a minor role of the lower to mid tropospheric water vapour distribution and the specific model set-up of air parcel release at locations close but below the tropopause. Although this approach has been successfully applied to answer many questions related to the water vapour distribution in the TTL (Schoeberl and Dessler, 2011; Schoeberl et al., 2012, 2013, 2014; Zhang et al., 2016; Schoeberl et al., 2018, 2019; Wang et al., 2019), it has never been directly compared against other configurations that consider the whole troposphere as well. This implies another source of uncertainty that might affect the water vapour simulation.

Another relevant process to the water vapor budget is ice microphysics (in particular, sedimentation and detrainment) in the UTLS related to the formation of cirrus clouds. Ice could be convectively lofted (Corti et al., 2008; Dessler et al., 2007, 2016; Ueyama et al., 2018; Wang and Dessler, 2012) or in situ formed (Wang and Dessler, 2012; Ploeger et al., 2013; Krämer et al., 2020). In the first case, it is not clear whether evaporation of ice injected into the LS by overshoots leads to a moistening of the LS (Corti et al., 2008; Wang and Dessler, 2012) or not (Ueyama et al., 2018). In the second case, cirrus clouds form in cold regions of the UTLS (Gettelman et al., 2002a), decreasing the water vapour present. However, depending on their properties such as their thickness cirrus clouds could lead to a warming of these regions Krämer et al. (2020). This agrees with Ploeger et al. (2013), which showed from model simulations that evaporation of ice in the UTLS increases the water vapour everywhere, including the Asian Monsoon region. However, the relative role of this microphysical process in contrast with other mechanisms not only on net water vapour in monsoon anticyclones but also on its variability, has not been assessed yet.

Turbulence and the associated small-scale mixing results in diffusivity in the UTLS, which affects the transport of trace gas constituents, including water vapour, into the LS (Podglajen et al., 2017). Konopka et al. (2007) showed that a parameterization of the small-scale mixing between nearby air masses based on the strain- and shear- induced deformation of the large-scale flow led to an enhancement of cross-tropopause transport in the monsoon regions and in particular in the Asian Monsoon. This mechanism has been invoked to explain observed tracer distributions in the UTLS (Pan et al., 2006). As flow deformation is commonly found in the vicinity of the subtropical jet stream, which is very close to the tropopause, air masses tend to mix in these regions. As a consequence, they reach the LS with higher water vapour content, avoiding in some cases the coldest temperatures of the tropopause (Poshyvailo et al., 2018). However, as reported by Poshyvailo et al. (2018) and Riese et al. (2012), the final impact of mixing on water vapour largely depends on the mixing strength predefined in their simulations and is thus highly uncertain.

At mid-stratospheric levels, methane oxidation acts as a source of water vapour. Through the downwelling branch of the Brewer–Dobson circulation, these moistened air masses get transported into the LS and partly are transported further into the

https://doi.org/10.5194/acp-2020-1010
Preprint. Discussion started: 27 October 2020


Atmospheric Chemistry and Physics Discussions

tropics, following the residual circulation (Ploeger et al., 2013). Despite the fact that this horizontal transport is not as strong as in the opposite direction, it has a non-negligible impact on the monsoon regions.

In this study, we use the Chemical Lagrangian Model of the Stratosphere (CLaMS) (McKenna et al., 2002b, a; Konopka et al., 2004) with the aim of describing and quantifying the contributions of the different physical processes to the water vapour distribution in the lower stratosphere and particularly over the Asian and American monsoons. For this purpose, we have performed five experiments to analyse the role of each of the following processes: large-scale temperatures, methane chemistry, ice microphysics, small-scale mixing processes, and in particular vertical tropospheric mixing (likely related to convection). Furthermore, we also assess the sensitivity of the LS water vapour signal to the domain-filling technique developed by Schoeberl and Dessler (2011), configuring all the experiments with this set up and comparing them with a long multi-decadal standard CLaMS simulation used in Konopka et al. (2004); Diallo et al. (2018); Tao et al. (2019). Besides, we used satellite observations from the Aura MLS v4.2 experiment, to assess the realism of each simulation. In Section 2, we introduce the domain-filling technique, the data and the configuration of the different experiments. In Section 3, we present the performance of each experiment in simulating LS water vapour and how they capture the variability of this signal over the Asian and North American monsoon regions. Finally, in Section 4, we discuss the relevance of the processes to explain the water vapour signal and also the differences in water vapour found using the domain-filling technique and the standard version of CLaMS.

2 Data and methodology

2.1 The CLaMS model

To evaluate the sensitivity of lower stratospheric water vapour over monsoon regions to different physical processes, we use the Chemical Lagrangian transport model CLaMS (McKenna et al., 2002b; Konopka et al., 2004). This model simulates the three-dimensional trajectories of an ensemble of air parcels forward in time, as well as the changes in the chemical composition of the air parcels along them. CLaMS has a modular structure that allows different parameterizations or new configurations to be easily implemented. Thus, the sensitivity of the water vapour distribution in the LS during boreal summer can be studied easily by switching on and off the parameterizations available in CLaMS.

The CLaMS model has been widely used to study the distribution of several tracers in the stratosphere (Riese et al., 2012), including recent studies on water vapour in the lower stratosphere (Tao et al., 2019; Poshyvailo et al., 2018). Previous studies have shown that the model properly simulates the variability of the stratosphere water vapour (Diallo et al., 2018; Tao et al., 2019) and the water vapour distribution over monsoon regions during boreal summer (Poshyvailo et al., 2018), highlighting the efficiency of these regions to transport air masses and water vapour into the TTL (Ploeger et al., 2017; Nützel et al., 2019; Yan et al., 2019).

All experiments performed for the present study use 6-hourly winds and temperature from the European Centre of Medium-range Weather Forecast (ECMWF) ERA-Interim reanalysis (Dee et al., 2011). The model uses a vertical hybrid coordinate that follows the orography with a σ-coordinate at the ground that transforms into potential temperature in the upper troposphere. Above σ=0.3 (about 300 hPa in regions without strong orography), the vertical coordinate is purely isentropic. Cross-isentropic

https://doi.org/10.5194/acp-2020-1010
Preprint. Discussion started: 27 October 2020


Atmospheric Chemistry and Physics Discussions

transport is simulated using total diabatic heating rates (considering all-sky radiation, latent heat release, diffusive and turbulent heat transport as detailed by Fueglistaler et al. (2009)) from ERA-interim forecast data, as described in Ploeger et al. (2010). For the sake of the analysis, simulated water vapour content of air parcels is daily regridded into maps with bin size 5°-longitude x 2°-latitude at a given pressure or potential temperature level with a thickness of 10 hPa or K, respectively. Hence, daily distributions of water vapour at 100 hPa are result of averaging air parcels found between 105 and 95 hPa.

2.2 Domain filling set up

To create a common framework between previous studies focusing on water vapour simulation (Schoeberl et al., 2013; Zhang et al., 2016; Wang et al., 2019) and our CLaMS sensitivity experiments, we have implemented the forward domain-filling technique, here referred as Lagrangian Trajectory Filling (LTF), into CLaMS. This set-up, described by Schoeberl and Dessler (2011), has been widely used to study different properties of water vapour in the stratosphere and UTLS region (Schoeberl et al., 2012, 2013, 2014; Dessler et al., 2014; Zhang et al., 2016; Ye et al., 2018; Schoeberl et al., 2018, 2019). The stratosphere is filled with air parcels which are released every day at a launch level and transported forward in time till they are filtered out of the simulation. This removal occurs when an air parcel reaches above 1800 K (considered as the top of the stratosphere) or below 250 hPa (return to the troposphere). At the beginning of the experiment, the total number of air parcels in the simulation increases with time due to the continuous release of new air parcels at the launch level. Then, after a spin-up time, the filtering-out balances the release rate, so that the total number of air parcels reaches an equilibrium value (∼500.000 air parcels in Schoeberl and Dessler (2011)).

In our experiments, we closely follow the set-up of Schoeberl and Dessler (2011), with air parcels being released on a homogeneous 5°-longitude x 2°-latitude grid covering all longitudes in the latitudinal range 60°S–60°N. As the level of initialization, we choose the potential temperature level θ=360 K, which is, on average, above the level of zero radiative heating (LZRH) (Gettelman et al., 2002a) but below the tropical tropopause (∼375–380 K). Our simulations encompass the period from 2005 to 2016. The equilibrium number of air parcels is generally reached after 2 years of simulation. Some experiments show larger values of the number of air parcels simulated per day than the achieved by Schoeberl and Dessler (2011), due to the direct impact of some parameterizations on these quantity (i.e, small-scale mixing).

2.3 Experiments

We performed five LTF experiments with CLaMS. A summary of all experiments is provided in Table 1. This set of experiments is configured in such a way that the tested parameterizations are added cumulatively, increasing the complexity and realism of the simulations step by step. The first experiment, hereafter called TRAJ, consists in purely advective trajectories launched at $\theta = 360$ K. It sets the start point of our experiments and does not include any parameterization. This basic configuration of CLaMS simulates the transport of air masses without changing their tracer composition along the path and thus, the water vapour simulated by this experiment corresponds to the Lowest Mixing Ratio (LMR) encountered by each air parcel along its trajectory. Mixing ratios are estimated following Murphy and Koop (2005).

https://doi.org/10.5194/acp-2020-1010
Preprint. Discussion started: 27 October 2020


Atmospheric Chemistry and Physics Discussions

In the second experiment, CHEM, the moistening effect of methane oxidation is added by applying the CLaMS chemistry module (Pommrich et al., 2014). Only chemical reactions that affect water vapour due to methane oxidation are included in this experiment. These reactions play a relevant role in the middle and upper stratosphere as a source of water vapour. As we allow the experiment to change the water vapour content of the air parcels, we have to initialize the ensemble of air parcels both with water vapour (50 ppmv) and methane (1.7 ppmv) concentrations, following Schoeberl et al. (2013). For the CHEM simulation, the CLaMS dehydration scheme (for details see Von Hobe et al., 2011) is configured equivalently to the LMR calculation in the basic TRAJ case. Therefore, an air parcel is set to saturation whenever its water vapour content is above 100% of relative humidity (RH), following Marti and Mauersberger (1993), which is similar to Murphy and Koop (2005). Then, it assumes instantaneous fall-out of all ice particles, removing water vapour in excess from saturation.

The third experiment, CIRRUS, applies the same initialization, simplified chemistry and dehydration scheme as CHEM, but in case of supersaturation, water vapour in excess is instantaneously transferred to the ice phase, instead of being removed, as described in Von Hobe et al. (2011). Then, a mean ice particle size and the corresponding settling velocity are computed using an empirically defined ice particle density based on in situ observations (Krämer et al., 2009). The consequent sedimentation length of the ice particles is compared to a characteristic length ($\sim$300 m, optimized by Ploeger et al. (2013)) to determine the fraction of ice removed from the simulation. If during the following time steps an air parcel turns out to be subsaturated and ice exists, then ice evaporates till the air parcel reaches saturation. Thus, this experiment considers the effect of the so-called in situ cirrus (Krämer et al., 2020) forming in supersaturated regions.

One of the key features of the CLaMS model is its parameterization of small-scale mixing processes (McKenna et al., 2002b; Konopka et al., 2004, 2007). This parameterization has been proposed to improve the simulation of tracer distributions in regions where large-scale deformations take place (Konopka et al., 2004; Pan et al., 2006; Konopka et al., 2007). As a first step, the mixing procedure considers the positions of the air parcels as nodes of a three-dimensional grid. During the advection step, the relative positions of those nodes change depending on the deformation of the background flow $\nabla\mathbf{u}$. Finally, a threshold distance is defined to establish whether the air parcels encounter mixing or not. If the distance between two nearest-neighbour parcels has increased (decreased) above (below) this threshold value because of the deformation of the flow, a new air parcel is inserted between the parcels involved in the mixing process (parcels involved are merged). The chemical composition of the new air parcel, i.e water vapour and methane, is set to the average of the mixing ratio of the parcels that experienced mixing. The threshold distance depends on the separation between air parcels before the advection step, the ratio between horizontal and vertical diffusivities, the regridding frequency (here once per day) and the critical Lyapunov exponent λ_c (here set to 0.5), which is chosen as a free parameter and controls the mixing strength (further details can be found in McKenna et al. (2002b), Konopka et al. (2004), Konopka et al. (2007) and Poshyvailo et al. (2018)). The fourth experiment, SSMIX, adds the small-scale mixing parameterization of CLaMS to the processes represented in CIRRUS. Once mixing has occurred, the same dehydration scheme as in CIRRUS is applied again to remove the supersaturation potentially introduced in new air parcels.

The fifth experiment, called VMIX, includes a new scheme to consider enhanced tropospheric mixing recently developed by Konopka et al. (2019). Whereas the previously described scheme considered quasi-isentropic mixing in regions with horizontal strains and vertical shears, this additional parameterization describes tropospheric mixing likely related to unresolved convec-

https://doi.org/10.5194/acp-2020-1010
Preprint. Discussion started: 27 October 2020

Atmospheric Chemistry and Physics Discussions

tive updrafts absent from the reanalysis wind fields. With VMIX, air parcels with a Brunt–Väisälä frequency, N^2, greater than a predefined value, N_c^2, undergo tropospheric mixing with their nearest neighbours. In other terms, their chemical composition is changed to the averaged mixing ratios of all the parcels involved in the mixing process. As a difference to the small-scale mixing scheme, this procedure does not change the position of the air parcels. To cover mixing caused by convective updrafts, the moist Brunt–Väisälä frequency N_m^2 is interpolated to the position of the air parcels. Whenever a conditionally unstable air parcel (N_m^2 <0) is detected, the air parcel position in the vertical coordinate is increased at least by 35 K. Therefore, if an air parcel encounters N_m^2>0 and $\Delta\Theta$>35 K, its position is changed in the vertical coordinate as if convection would have triggered vertical motion. Further details of this parameterization and its validation with proxies of deep convection (OLR) can be found in Konopka et al. (2019).

Finally, we consider the standard climatological simulation of CLaMS (STANDARD) (Diallo et al., 2018; Tao et al., 2019) as the sixth experiment in our study. This climatological run considers the same ensemble of parameterizations applied in SSMIX, with the exception of the LTF scheme. The air parcels are released at the beginning of the simulation in the middle of each vertical layer filling up both the troposphere and stratosphere and using a horizontal separation corresponding to the model horizontal resolution (100 km). Once released, trajectories of air parcels are computed using reanalysis horizontal wind fields and diabatic heating rates for vertical transport. When air parcels are in the troposphere below about 500 hPa, their the water vapour content is interpolated from ERA-interim while methane is derived from ground-level observations. The CLaMS dehydration and chemistry schemes are applied, configured consistently with the CIRRUS experiment. In opposition to the LTF technique, no air parcel is filtered out of the experiment below 250 hPa or above 1800 K and the water vapour content of air parcels at 360 K is not fixed uniformly to 50 ppmv. Here we will refer to this set up as "Stratosphere-Troposphere Filling" (ST-Filling). Further details of the initialization can be found in McKenna et al. (2002b, a), Konopka et al. (2004) and Pommrich et al. (2014).

2.4 Aura MLS observations

Satellite observations of water vapour mixing ratios in the LS from Aura Microwave Limb Sounder (Waters et al., 2006) experiment are used to assess the realism of our experiments. We use the version 4.2 of the water vapour data from MLS (Lambert et al., 2015) which has been fully described in (Livesey et al., 2018). These water vapour products have been validated in several studies and recently have been part of a climatological overview of the Asian Monsoon (Santee et al., 2017). Here, Aura MLS data and CLaMS data have been compiled on the same regular latitude-longitude grid.

3 Results

3.1 Lower stratospheric water vapour distributions

Figure 1 (left column) depicts the climatological water vapour distribution at 100 hPa during June-July-August (JJA) and over the period 2007–2016 as represented by the different CLaMS experiments and MLS observations. Results reveal that all

https://doi.org/10.5194/acp-2020-1010
Preprint. Discussion started: 27 October 2020


Atmospheric Chemistry and Physics Discussions

experiments with the LTF scheme (Fig. 1b–f) successfully simulate the main characteristics of the water vapour distribution found in MLS. From the most basic to the most complex configurations (from TRAJ to SSMIX), they all reproduce the contrast between the driest regions, located over the tropics and subtropics, and mid-high latitudes, where humidity strongly increases. Also, in the northern hemisphere, they show the maximum in the Asian Monsoon Anticyclone (AMA), as it is found in MLS. However, there are also some important differences in relation to the spatial pattern. In comparison with MLS (Fig. 1a), experiments with the LTF scheme (Fig. 1b–f) tend to underestimate the water vapour content of the lower stratosphere over most regions. In the case of TRAJ, the most basic configuration, the water vapour content is between 1.5 and 2 ppmv lower than for MLS. These differences decrease as the experiments become more complex and include new parameterizations that bring them closer to the observations. In addition there is a misrepresentation of the North American Monsoon Anticyclone (NAMA) for which all experiments tend to show a weaker maximum shifted towards the eastern and central Pacific with respect to observations.

In order to show the contributions of each parameterization to the climatology, Figure 1 (right column) exhibits the differences between pairs of experiments sharing the same configuration except for one parameterization. In this way, we isolate the effect of each parameterized physical process on the water vapour distribution in the LS. Following this approach, we compute CHEM minus TRAJ differences in order to isolate the effect of methane oxidation (Fig. 1h) since, as shown in Table 1, these two experiments share the same configuration except the methane oxidation scheme, which is only included in CHEM. Following the same procedure we compute the differences between CIRRUS and CHEM, SSMIX and CIRRUS and VMIX and SSMIX to isolate the effects of the cirrus parameterization (Fig. 1i), small-scale vertical mixing (Fig. 1j) and enhanced tropospheric mixing (Fig. 1k), respectively.

Regarding methane oxidation, Figure 1h shows a water vapour increase of around +0.1 ppmv over the tropics and subtropics that reaches +0.2 ppmv over high latitudes. As methane oxidation occurs at mid-stratospheric levels, its impact on the water vapour distribution at 100 hPa (Fig. 1h) is a consequence of air parcels moving downward from those altitudes following the down-welling branch of the Brewer–Dobson circulation at high latitudes. During boreal summer, the downward circulation is stronger in the southern hemisphere, which explains the larger increase of water vapour in this region. Once air parcels reach the lower stratosphere at high latitudes, some of them may reach the troposphere below 250 hPa, where they are removed from simulation, while others follow the residual meridional circulation giving rise to the observed subtropical and tropical enhancements of water vapour at 100 hPa. This weak meridional transport was also observed by Ploeger et al. (2013) and Poshyvailo et al. (2018). A similar impact of methane oxidation has been found at 80 hPa in spite of the stronger meridional gradient at this pressure level (Fig. A1).

The comparison between figures 1i and 1h reveals that ice microphysics is responsible for a stronger moistening of the LS than that attributed to methane, giving rise to a water vapour increase ranging between +0.4 ppmv and +0.6 ppmv over most regions. These values are in agreement with the global increase of +0.5 ppmv found by Ploeger et al. (2013). However, Figure 1i shows that the effects of ice are especially large in the AMA, where it involves an increase of almost +0.8 ppmv at 100 hPa. This pattern is also found at 80 hPa but with slightly weaker values than those at 100 hPa (Fig. A1i).

https://doi.org/10.5194/acp-2020-1010
Preprint. Discussion started: 27 October 2020


Atmospheric Chemistry and Physics Discussions

Small-scale mixing has a similar impact (Fig. 1j), increasing water vapour at latitudes north of 30°S and especially over the Asian Monsoon. Excluding its effect in the AMA, the water vapour increase linked to small-scale mixing is slightly weaker than that attributed to ice microphysics (Fig. 1i), ranging between +0.1 and +0.4 ppmv. In contrast, its impact on water vapour in the Asian Monsoon is stronger, reaching values of +0.9 ppmv at 100 hPa. This can be attributed to the fact that, in the upper troposphere, mixing processes are more frequent over regions with large-scale flow deformations, which mainly located in the surroundings of the subtropical jet (Konopka and Pan (2012), Poshyvailo et al. (2018)) and hence over the Asian Monsoon. Furthermore, small-scale mixing allows the mixing of air parcels at different pressure levels in the UTLS, bypassing cold traps encountered during horizontal advection. In this case, water vapour could be transported to higher altitudes avoiding the CPT and giving rise to an increase of water vapour over most regions, but especially where the mixing is stronger. The 80 hPa level shows a similar spatial distribution of water vapour differences to that at 100 hPa, with values peaking again in the AMA (Fig. A1j). However, the relative strength of this maximum (+0.5 ppmv) is here weaker than at 100 hPa.

Figure 1k shows the changes attributed to the enhanced mixing in the troposphere considered in VMIX. Here one should be aware of the fact that the LTF scheme filters out the air parcels below 250 hPa. Therefore, the effect of the enhanced tropospheric mixing is limited to upper tropospheric levels, so that the simulation of convective updrafts is substantially suppressed. Even in this case an increase in water vapour of up to +0.1 ppmv occurs almost everywhere north of 30°S, with a relatively higher impact over the Asian Monsoon, where differences reach values above +0.3 ppmv. This stronger influence in the AMA in comparison to other regions is also found at 80 hPa but weaker than at 100 hPa. Although we expect that this impact mainly originates from tropospheric mixing processes, we cannot completely exclude the effect of convective updrafts, as the parameterization may account for either one or the other, or both processes. Therefore, it is not certain which of the two processes here considered, tropospheric mixing or convective updrafts, is playing a major role, neither at 100 hPa nor at 80 hPa. Compared to other processes, VMIX shows a weak increase of water vapour in the AMA related to the enhanced tropospheric mixing, including turbulence and convective updrafts. Apparently, this is not consistent with Ueyama et al. (2018); Wang et al. (2019) that highlight the importance of convection to reproduce the monsoonal maxima of water vapour. However, it is highly likely that the effect of convective updrafts is very limited by the filtering of air parcels below 250 hPa in our LTF set-up. Thus, it is possible that if lower tropospheric levels were taken into account, convective updrafts would be better simulated and could result in a greater moistening of the LS than the one simulated here.

Finally, we assess the sensitivity of the LS water vapour to the LTF scheme. For this purpose, we analyse the water vapour fields of the sixth experiment, STANDARD, which uses the same parameterizations as SSMIX, but calculates transport throughout the entire troposphere, and which water vapour initialized with ERAinterim values in the lower to mid troposphere. Thus, contrary to the LFT scheme, no air parcels are filtered out below 250 hPa or above 1800 K and the water vapour content of the air parcels at 360 K depends on the transport properties of the air parcels reaching that altitude. Figure 1g and l depict the water vapour distribution obtained for the STANDARD simulation and its differences with respect to SSMIX, respectively. The STANDARD simulation exhibits a much wetter stratosphere than SSMIX, which leads to a weak overestimation of the water vapour and in particular in the AMA, compared to MLS. However, the main differences caused by the LTF scheme are not centered over the Asian Monsoon region but over both Western and Eastern parts of the North Pacific and between a

https://doi.org/10.5194/acp-2020-1010
Preprint. Discussion started: 27 October 2020


Atmospheric Chemistry and Physics Discussions

longitudinal band centered between 20°–30°S. At 80 hPa, those differences are registered at the same latitudes and expanded zonally. This implies that the global effect of the LTF set-up is to dry the stratosphere in comparison with the STANDARD simulation, but in particular at the edges of the tropical pipe with smallest differences in the AMA.

Concerning the North American Monsoon, we found that its spatial pattern is not well reproduced in any of the experiments (Fig. 1). The region of the maximum is shifted to the west and, except in the STANDARD simulation, which shows water vapour values in the NAMA close to the observations, all other experiments display much lower values.

3.2 Variability of water vapour over monsoon regions

3.2.1 Seasonal variability

Figure 2 shows the annual cycle at 82 hPa (top) and 100 hPa (bottom) of the simulated and observed water vapour over the Asian (left column) and North American monsoons (right column), averaged over the period 2007–2016. In both regions and at both pressure levels, all experiments represent the observed increase of water vapour during boreal summer. As expected, the peak water vapor is delayed by 1–2 months delay at 82 hPa with respect to 100 hPa. In agreement with Fig. 1, Figs. 2a and b show that the LTF experiments tend to underestimate water vapour over the Asian Monsoon in comparison with MLS values. Thus, the lowest water vapour values are obtained with TRAJ and CHEM, while SSMIX and VMIX better match the observations. Figure 2a and b reveal that CIRRUS as well as SSMIX and VMIX show a steeper water vapour increase between June and August than CHEM and TRAJ, resulting in a better agreement with MLS during the monsoon season (particularly pronounced at 100 hPa). In the case of CIRRUS, this is consistent with observations of cirrus clouds linked with the large-scale convection developing during these months (Ueyama et al., 2018; Krämer et al., 2020). On the other hand, in the case of SSMIX and VMIX, both experiments show a sharp increase of water vapour in June, which is stronger than in the observations and results in values close to MLS at 100 hPa during July and August. This increase is weaker at 80 hPa, where water vapour values remain well below MLS. This feature at both pressure levels points out the role of mixing processes in this region, in particular those processes represented by the small-scale mixing parameterization. The differences between VMIX and SSMIX show a slight increase of water vapour linked with the enhanced tropospheric mixing scheme applied in VMIX. The larger differences to SSMIX during the monsoon season point to an effect of the enhanced convective updrafts in the monsoon region during summer.

Finally, the STANDARD simulation, the only one without the LTF set-up, matches best the observed annual cycle of the water vapour in the AMA at 100 and 82 hPa, providing evidence that the use of the LTF set up causes the lower stratosphere to be dry biased compared to observations. On the other hand, the STANDARD simulation results in a slight overestimation of water vapour that is larger at 100 hPa during the mature phase of the Asian Monsoon. This weak overestimation is likely related to the stronger water vapour increase at the beginning of the monsoon season for this experiment (and also for SSMIX and VMIX).

Despite the differences between the simulated and observed water vapour distributions over the North American Monsoon, all experiments show a seasonal cycle consistent with MLS (Figs. 2c). This figure also shows that, as for the Asian Monsoon,

https://doi.org/10.5194/acp-2020-1010
Preprint. Discussion started: 27 October 2020


Atmospheric Chemistry and Physics Discussions

humidity remains below observed values in all LTF experiments. However, in contrast to the Asian Monsoon, this underestimation of the water vapour mixing ratios becomes larger between June and August, since the observed values increase significantly faster between May and July. In addition, contrary to the Asian Monsoon, the effects of the non-removal of ice and small-scale mixing are quite uniform throughout the year, not showing any intensification during the monsoon season. The lower stratosphere for both SSMIX and VMIX is wetter than for CIRRUS, the wettest for VMIX. However, the three experiments remain very close to each other over the year, which reflects the minor impact of small-scale mixing processes in the NAMA, as compared to the Asian monsoon. As previously mentioned, small-scale mixing depends on deformations of the large-scale flow. The North American Monsoon is known to show a less confined large-scale circulation (Gettelman et al., 2004), which could render this region more sensitive to overshooting convection (not included in our experiments with CLaMS) in comparison with the Asian Monsoon. Finally, as in the case of the Asian Monsoon, the STANDARD simulation shows water vapour values closest to the observations at both pressure levels (Fig. 2b and c). However, the STANDARD simulation overestimates MLS values in the North American monsoon from October to May and shows a weaker water vapour increase at the beginning of the monsoon season resulting in an underestimation of the humidity during the monsoon period, in line with the results obtained for the LTF experiments.

3.2.2 Subseasonal variability

In order to assess the representation of the water vapour variability over the Asian Monsoon besides the seasonal cycle, Figure 3a–f depicts deseasonalized daily anomalies of water vapour during 2007–2016 for each experiment and MLS observations together with the respective correlations. With the aim of analysing the experiment's performance during the entire monsoon season (from May to September, MJJAS) and during the months corresponding to the mature phase of the monsoon season (June-July-August, JJA), these correlations are computed for both periods. Results show that all LTF experiments reach statistically significant correlations, which increase with the complexity of the experiment. Thus, the lowest values are obtained for the simpler configurations, TRAJ and CHEM ($r=0.51/0.62$ for JJA/MJJAS, $p<0.025$). However, the fact that even the TRAJ experiment correlates relatively well with the observations supports the idea that cold point temperature variability is the main driver of LS water vapour variability over the Asian Monsoon. Furthermore, these results reveal that methane oxidation is irrelevant to water vapour variability in the AMA. On the other hand, including a simple parameterization of in situ ice formation and evaporation slightly improves the correlation during both JJA and MJJAS, but this improvement is much higher when small-scale mixing processes are considered. Thus, among the LTF experiments, the highest correlations are obtained for SSMIX ($r=0.64/0.69$ for JJA/MJJAS , $p<0.025$) and VMIX ($r=0.65/0.68$ for JJA/MJJAS , $p<0.025$). This result manifests that, despite the overestimation of the water vapour increase at the beginning of the monsoon season caused by the parameterization of the small-scale mixing processes found in Fig. 2a and b, mixing significantly contributes to the simulation of a more realistic water vapour variability over the Asian Monsoon. The comparison of the results obtained for SSMIX and VMIX shows that the enhanced tropospheric mixing scheme, which only has a mild impact on the water vapour distribution (Fig. 1f and k), does not improve the simulation of water vapour variability over the Asian Monsoon.

https://doi.org/10.5194/acp-2020-1010
Preprint. Discussion started: 27 October 2020


Atmospheric Chemistry and Physics Discussions

Finally, Figure 3f shows evidence that, for both sets of months, the STANDARD simulation correlates best with MLS, reaching values of 0.76 and 0.74 ($p<0.025$) for JJA and MJJAS, respectively and significantly improving the correlations. This means that the use of an LTF scheme involves not only a strong dehydration of the LS, but also a lack of intra-seasonal variability in the Asian Monsoon. The possible mechanisms behind these results are discussed in Section 4.

Figure 3g–l shows that simulated deseasonalized daily anomalies of water vapour over the North American Monsoon correlate relatively well with MLS for both sets of months, reaching even higher correlations than over the Asian Monsoon. The STANDARD simulation shows the highest correlation with MLS ($r=0.83$, $p<0.025$ in JJA) followed by the LTF experiments that includes the small-scale mixing parameterization (SSMIX, 0.78 and VMIX 0.77 in JJA). The lowest correlation is achieved by TRAJ ($r=0.73$ in JJA), which is very similar to the highest correlation achieved in the Asian Monsoon case. As TRAJ experiment achieves high correlation values with MLS, which are not so far from the rest of the experiments, this indicates that temperature is the main controller of intra-seasonal variability in the NAMA, with the other processes considered here being less important. The reason why correlations in the NAMA are higher than in the AMA, is likely related to the fact that other processes play a larger role when the large-scale anticyclonic circulation and related confinement are strong enough, as in the AMA.

4 Discussion and conclusions

In this study, we compare five experiments in order to assess the impact of large-scale temperatures, methane oxidation, ice microphysics, small-scale mixing and enhanced tropospheric mixing on the lower stratosphere (LS) water vapour distribution and, in particular, over the Asian and North American Monsoon Anticyclones, AMA and NAMA respectively. These experiments share the same set-up based on the domain filling technique developed by Schoeberl and Dessler (2011) (here called Lagrangian Trajectory Filling, LTF, see Section 2.2), while the parameterization of each chemical or physical process aforementioned is included cumulatively (Table 1). In a first step, we discuss the effects of ice microphysics and small-scale atmospheric mixing processes on moistening the LS. In a second step, we evaluate the sensitivity of our results to the initialization scheme (LTF), by comparing the pure trajectory model experiments to a sixth experiment (STANDARD) configured using the here-called "ST-Filling" (see Section 2 and McKenna et al. (2002b, a); Pommrich et al. (2014) for further details).

4.1 Moistening of the LS by ice microphysics and small-scale mixing

Our results show that TRAJ experiment, which estimates water vapour values only through the LMR, can already reproduce some of the observed characteristics of the water vapour distribution in the LS such as the latitudinal variations and the maximum in the AMA. The relatively good performance of this experiment is consistent with the key role of the Cold Point Tropopause (CPT) in controlling the LS water vapour distribution. Nevertheless, this experiment underestimates the water vapour content of the LS by about 1.5 to 2 ppmv compared to MLS observations, which evidences that temperature alone is not able to explain the LS water vapour content and points to the necessity of considering additional processes. Regarding the North American Monsoon, this experiment shows a water vapour maximum over the eastern Pacific that is shifted to the

https://doi.org/10.5194/acp-2020-1010
Preprint. Discussion started: 27 October 2020


Atmospheric Chemistry and Physics Discussions

west compared to MLS (where the maximum is located in the monsoon region). This is a common characteristic in all the experiment of this study and could be related to the lack of a convective transport scheme, as has already been pointed out by Nützel et al. (2019).

Our results confirm the importance of the parameterization of ice microphysics which, in our CIRRUS experiment, is responsible for an increase of water vapour in the LS during boreal summer. When an air parcel travels through supersaturated conditions, its water vapour in excess of saturation is converted into ice. The ice then sediments out with a finite settling velocity. Thus, the ice is only partially removed for certain conditions and may evaporate at later time steps if the air parcel travels back to subsaturated regions. With our simplified microphysical scheme, this process results in an global average increase of water vapour of around 0.5 ppmv with a stronger impact over the Asian Monsoon (+0.8 ppmv), consistent with the higher amount of cirrus clouds and a higher frequency of supersaturation conditions in the AMA (Krämer et al., 2020). On the contrary, this process is not particularly strong over the North American Monsoon region. It should be kept in mind that in situ formation, as represented here, is only one of the many processes through which ice influences the water vapour content. Ice is also formed at lower altitudes and transported to the UTLS by deep convection, reaching during strong overshooting events the LS and evaporating afterwards. We expect that these processes not included in our simulations would increase the moistening effect.

Regarding small-scale mixing, the SSMIX experiment shows that this process can give rise to a water vapour increase that reaches 0.9 ppmv over the Asian Monsoon. This moistening effect is in agreement with previous studies showing that the effect of small-scale atmospheric mixing processes is particularly important over the Asian monsoon region due to the strong deformation of the flow caused by the subtropical jet stream (Konopka et al., 2007; Poshyvailo et al., 2018). This moistening effect is much weaker over the North American Monsoon, which suggests that the weaker anticyclonic monsoon circulation over that region produces a weaker deformation of the main flow leading to less mixing between air masses.

Concerning the variability of the simulated water vapour over the Asian Monsoon, our results show that the "no mixing" experiments (TRAJ, CHEM and CIRRUS) can reproduce the annual cycle with a maximum during the boreal summer in agreement with MLS observations. These experiments achieve correlations slightly above 0.6 between their deseasonalized anomalies and those of MLS for the MJJAS months. However, small-scale mixing experiments show an important improvement in simulating both the annual cycle and the intra-seasonal variability at 100 hPa during the central monsoon season (JJA), when the correlations between “no mixing” experiments and MLS decrease to values slightly above 0.5. In contrast, mixing experiments (SSMIX, VMIX and STANDARD) keep their correlations with MLS at similar values for JJA and MJJAS. We conclude that in the mature phase of the monsoon, the dominant role of the temperature on water vapour is weakened compared to other processes that trigger mixing between air parcels.

In the case of the North American Monsoon, all experiments reproduce a similar seasonal variability with a slight delay in the timing of the water vapour maximum with respect to MLS. None of the processes here considered seems to be particularly relevant for the NAMA. Furthermore, all the experiments show similar correlation values of around 0.7 for the deseasonalized anomalies of water vapour independently of the chosen months (MJJAS or JJA). This emphasizes that the variability of water

https://doi.org/10.5194/acp-2020-1010
Preprint. Discussion started: 27 October 2020


Atmospheric Chemistry and Physics Discussions

vapour over this region on both seasonal and intra-seasonal timescales is largely explained by temperatures, even during the mature monsoon phase (JJA).

Finally, we found that the impact of the methane oxidation in the tropics is weak, in agreement with Ploeger et al. (2013), and indifferent to the transport properties of the monsoon regions.

4.2 Sensitivity of water vapour to LTF

One of the aims of this study is to analyse the effect of the initialization scheme on the simulation of the LS water vapour through the comparison of the STANDARD simulation with the SSMIX (LTF) experiment. Our results show that STANDARD simulates a wetter LS than SSMIX and that, in spite of the overestimation of water vapour over certain regions, it is the experiment that best reproduces the seasonal cycle and the deseasonalized anomalies over the Asian and North American monsoons. The relative inaccuracy of the LTF experiments might be attributed to two features: i) the filtering of air parcels below 250 hPa and above 1800 K and ii) the initial water vapour content of the air parcels.

The first feature of the LTF set-up allows a balance between the number of new air parcels released per day and those filtered out of the simulation, as they leave the stratosphere. We found that this balance is achieved for a lower number of air parcels per day in SSMIX than in STANDARD and for even lower number in the rest of the LTF experiments without small-scale mixing (TRAJ, CHEM and CIRRUS, see Table 1). The number of air parcels might be irrelevant unless there is a bias by which the missing parcels in one experiment are not homogeneously distributed but tend to concentrate over regions with certain humidity characteristics. This is evident in Fig. A2, which shows exemplary the daily distributions of water vapour between 30 July and 4 August of 2013. The empty bins observed in this figure are, hereafter, named "gaps". These gaps appear when in the gridding process, in which air parcel positions are projected onto a map, certain bins remain empty. Figure A2 suggests that the gaps in SSMIX tend to concentrate over regions that are especially humid in STANDARD, as the AMA. Figure 4a shows the difference in the accumulated sum of gaps found during JJA between 2007 and 2016 between STANDARD and SSMIX. A larger sum of gaps is found over the AMA and between 20°S–25°S for SSMIX than for STANDARD. Figure 4b shows the relative percentage of total air parcels simulated in STANDARD with respect to SSMIX. Everywhere, STANDARD registers more air parcels than SSMIX, as the difference is always larger than 100%. Maxima occur over the regions of the Asian monsoon and of the SH subtropics (Fig. 4b). This result suggests that LTF does not fill up the stratosphere uniformly leading to a lack of air parcels particularly in areas with a higher water vapour content such as the Asian Monsoon (Fig. 1g), partially explaining the drier conditions in SSMIX compared to STANDARD. Figure 4e shows (solid lines) the probability density distribution (PDF) of the water vapour content of bins in the AMA at 100 hPa, together with (dashed lines) the PDF of water vapour of empty bins (gaps) inside the AMA region for STANDARD and SSMIX. The PDF of water vapour in the gaps of SSMIX was calculated from the water vapour distribution of the STANDARD simulation during JJA over the period 2007 and 2016. The fact that the PDF of these bins is shifted towards wetter values demonstrates that in SSMIX gaps are associated with events of high humidity transport through the AMA in STANDARD.

It is likely that small-scale mixing is smoothing the impact of the LTF scheme on water vapour as it adds new air parcels into the simulation whenever mixing occurs. Figure 4c evidences that CIRRUS, a “no mixing” experiment, shows a higher density

https://doi.org/10.5194/acp-2020-1010
Preprint. Discussion started: 27 October 2020


Atmospheric Chemistry and Physics Discussions

of gaps than SSMIX, which are also more frequent in the AMA. Figures 4c and d show that during JJA more gaps appear in CIRRUS with respect to SSMIX in particular in the AMA, consistent with CIRRUS showing a lower number of air parcels over this region. The comparison of the water vapor distribution of these two experiments reveals that particularly in the AMA the CIRRUS experiment exhibits much drier conditions than SSMIX (Fig. 1j). A link between the occurrence of gaps and drier conditions in the AMA exists if, in CIRRUS, these gaps tend to occur over those bins with a higher water content in SSMIX. This is precisely what Figure 4e shows. The green dashed line displays the SSMIX PDF of the water vapour content of the bins inside the AMA region that corresponds to gaps in CIRRUS. The higher water vapour content of these bins in comparison with the water vapour content of all the bins inside the AMA region (green solid line) demonstrates that CIRRUS gaps tend to appear associated to events of high humidity transport through the AMA in SSMIX and explains why the occurrence of these gaps gives rise to drier conditions in the AMA in CIRRUS. This result remarks that gaps found in CIRRUS, as a direct consequence of the LTF scheme, are partially filled up in SSMIX as result of the releasing of new air parcels by the small-scale mixing procedure, bringing water vapor values closer to observations.

It is possible that the lack of air parcels in LTF experiments is related to the level chosen for their release. Here, we are using the 360 K level and the anticyclonic circulation of the Asian Monsoon is likely already strong at that level, such that the inner anticyclone core is, to some degree, isolated from the surrounding areas. Given this scenario, only those air parcels directly released inside the core region of the Asian Monsoon anticyclone could be detected in this region also at higher altitudes, in agreement with Garny and Randel (2016). For the rest of the air parcels released in outer regions entrainment into the anticyclone core region would be inhibited. This would explain the lack of an impact exerted by the LTF scheme in the North American Monsoon, as the confinement caused by the anticyclonic monsoonal winds is weaker there. Another possible explanation might be the lack of various tropospheric levels in LTF experiments, which might act as a source of air parcels for large-scale convective processes in the Asian Monsoon. This would also explain why the STANDARD simulation reaches higher correlation values with MLS during JJA in Fig. 3f than LTF experiments and why mixing experiments (SSMIX and VMIX, Fig. 3d and f) correlate better than no mixing experiments (TRAJ, CHEM and CIRRUS, Fig. 3a, b and c). This suggests that the ST-Filling and small-scale mixing might help to simulate part of the variability linked with large-scale convective processes. It should be pointed out that an effect of small-scale mixing is to enhance cross-isentropic and cross-tropopause transport Konopka et al. (2004), which is the same effect as for convection. This might explain why SSMIX exhibits enhancements of water vapour very similar to the increase of water vapour linked with convection in the Asian Monsoon showed by Wang et al. (2019).

So far, we have analyzed the effects of the air parcel filtering. But, as previously mentioned, another characteristic of the LTF scheme that can have an impact on the LS water vapour distribution is the selection of the initial water vapour content of the air parcels that are released at the 360 K level (daily). To investigate this further, we compare the water vapour distributions at the 360 K potential temperature level for STANDARD and SSMIX in Fig. 5 (left column). As in all LTF experiments also in SSMIX the initial water vapour content of the air parcels is set to 50 ppmv. The figure also shows the observed water vapour distribution at 360 K from MLS for comparison to analyse the performance of both experiments. The STANDARD water vapor distribution agrees quite well with MLS and displays its main characteristic at this level: a strong moisture maximum in the

https://doi.org/10.5194/acp-2020-1010
Preprint. Discussion started: 27 October 2020


Atmospheric Chemistry and Physics Discussions

AMA. However, while this maximum reaches only 60 ppmv in MLS, in STANDARD it reaches values above 100 ppmv. In contrast, SSMIX exhibits a drier water vapour signal over the Asian Monsoon with maximum values below 30 ppmv. Figure 5 (right column) shows a correlation between the variability in these maximum values and the variability at each grid point in the global water vapour distribution at 100 hPa. Thus, the higher/lower values of this maximum probably contribute to the wetter/drier conditions of the LS at 100 hPa in STANDARD/SSMIX (Fig. 1g). To check if the water vapour content in the Asian Monsoon in LTF experiments depends on the initial water vapour content of air parcels, we perform an experiment configured as SSMIX but doubling the initial water vapour content of air parcels to 100 ppmv (SSMIX100 in Fig. 5). Our results reveal a clear moistening of the 360 K potential temperature level is observed, but far from 100 ppmv. This is likely a consequence of the dehydration scheme, which sets the water vapour content of the air parcels to saturated conditions. Besides, the water vapour distribution at 360 K is a result of newly released air parcels with air parcels already released in the past. Then, old dry air is present at this potential level, drying the 360 K. In any case, even when a clear moistening of 360 K is visible, the SSMIX100 water vapour distribution at 100 hPa does not change (Fig. A3). Thus, we conclude that water vapour in LTF experiments is not sensitive to the initial water vapour content of air parcels, as long as levels sufficiently far above the initialization level are considered. However, we suggest that the importance of the maximum found in the Asian Monsoon at higher altitudes might be related with transport processes in the troposphere which are represented in the STANDARD simulation by the ST-Filling set up but not in the LTF experiments. Hence, the simulated water vapour distribution in the UTLS, and in particular in the Asian monsoon region, is sensitive to the model lower boundary (e.g., for air parcel release in Lagrangian models), a fact to be further considered in the future.

Data availability. Data used for experiments are available upon request from authors NP (npplamar@upo.es) and FP (fploeger@fz.julich.de). MLS H2O version 4.2 data can be obtained from the MLS website https://mls.jpl.nasa.gov (last access: 28 August 2020).

Author contributions. NP, AP and FP designed the experiments. NP and AP performed the experiments with CLaMS. NP performed the data analysis. NP, CP, AP and FP contributed to the discussion of results. NP and CP wrote the text. CP, AP and FP made the final review.

Competing interests. The authors declare that they have no conflict of interest.

Acknowledgements. We would like to thank Bernard Legras for performing an experiment with TRACZILLA and share with us his work. We thank the Institute of Climate from the Research Center of Jülich and, in special, Martin Riese, for their scientific, technical and financial support. This research was funded by the Spanish Ministerio de Economía y Competitividad through the project Variabilidad del Vapor de Agua en la Baja Estratosfera (CGL2016-78562-P).

https://doi.org/10.5194/acp-2020-1010
Preprint. Discussion started: 27 October 2020

Atmospheric Chemistry and Physics Discussions

References

Corti, T., Luo, B., De Reus, M., Brunner, D., Cairo, F., Mahoney, M., Martucci, G., Matthey, R., Mitev, V., Dos Santos, F., et al.: Unprecedented evidence for deep convection hydrating the tropical stratosphere, Geophysical Research Letters, 35, 2008.

Dee, D. P., Uppala, S. M., Simmons, A., Berrisford, P., Poli, P., Kobayashi, S., Andrae, U., Balmaseda, M., Balsamo, G., Bauer, d. P., et al.: The ERA-Interim reanalysis: Configuration and performance of the data assimilation system, Quarterly Journal of the royal meteorological society, 137, 553–597, 2011.

Dessler, A. and Sherwood, S.: Effect of convection on the summertime extratropical lower stratosphere, Journal of Geophysical Research: Atmospheres, 109, 2004.

Dessler, A., Hanisco, T., and Fueglistaler, S.: Effects of convective ice lofting on H2O and HDO in the tropical tropopause layer, Journal of Geophysical Research: Atmospheres, 112, 2007.

Dessler, A., Schoeberl, M., Wang, T., Davis, S., Rosenlof, K., and Vernier, J.-P.: Variations of stratospheric water vapor over the past three decades, Journal of Geophysical Research: Atmospheres, 119, 12–588, 2014.

Dessler, A., Ye, H., Wang, T., Schoeberl, M., Oman, L., Douglass, A., Butler, A., Rosenlof, K., Davis, S., and Portmann, R.: Transport of ice into the stratosphere and the humidification of the stratosphere over the 21st century, Geophysical Research Letters, 43, 2323–2329, 2016.

Diallo, M., Riese, M., Birner, T., Konopka, P., Muller, R., Hegglin, M. I., Santee, M. L., Baldwin, M., Legras, B., and Ploeger, F.: Response of stratospheric water vapor and ozone to the unusual timing of El Niño and the QBO disruption in 2015–2016, Atmospheric Chemistry and Physics, 18, 13 055–13 073, 2018.

Fueglistaler, S. and Haynes, P.: Control of interannual and longer-term variability of stratospheric water vapor, Journal of Geophysical Research: Atmospheres, 110, 2005.

Fueglistaler, S., Bonazzola, M., Haynes, P., and Peter, T.: Stratospheric water vapor predicted from the Lagrangian temperature history of air entering the stratosphere in the tropics, Journal of Geophysical Research: Atmospheres, 110, 2005.

Fueglistaler, S., Legras, B., Beljaars, A., Morcrette, J.-J., Simmons, A., Tompkins, A., and Uppala, S.: The diabatic heat budget of the upper troposphere and lower/mid stratosphere in ECMWF reanalyses, Quarterly Journal of the Royal Meteorological Society: A journal of the atmospheric sciences, applied meteorology and physical oceanography, 135, 21–37, 2009.

Garny, H. and Randel, W. J.: Transport pathways from the Asian monsoon anticyclone to the stratosphere, Atmospheric Chemistry and Physics (ACP), pp. 2703–2718, 2016.

Gettelman, A., Randel, W., Wu, F., and Massie, S.: Transport of water vapor in the tropical tropopause layer, Geophysical research letters, 29, 9–1, 2002a.

Gettelman, A., Salby, M., and Sassi, F.: Distribution and influence of convection in the tropical tropopause region, Journal of Geophysical Research: Atmospheres, 107, ACL–6, 2002b.

Gettelman, A., Kinnison, D. E., Dunkerton, T. J., and Brasseur, G. P.: Impact of monsoon circulations on the upper troposphere and lower stratosphere, Journal of Geophysical Research: Atmospheres, 109, 2004.

Gill, A. E.: Some simple solutions for heat-induced tropical circulation, Quarterly Journal of the Royal Meteorological Society, 106, 447–462, 1980.

Hoskins, B. J. and Rodwell, M. J.: A model of the Asian summer monsoon. Part I: The global scale, Journal of the Atmospheric Sciences, 52, 1329–1340, 1995.

https://doi.org/10.5194/acp-2020-1010
Preprint. Discussion started: 27 October 2020

Kim, J., Randel, W. J., and Birner, T.: Convectively driven tropopause-level cooling and its influences on stratospheric moisture, Journal of Geophysical Research: Atmospheres, 123, 590–606, 2018.

Konopka, P. and Pan, L. L.: On the mixing-driven formation of the Extratropical Transition Layer (ExTL), Journal of Geophysical Research: Atmospheres, 117, 2012.

Konopka, P., Steinhorst, H.-M., Grooß, J.-U., Günther, G., Müller, R., Elkins, J. W., Jost, H.-J., Richard, E., Schmidt, U., Toon, G., et al.: Mixing and ozone loss in the 1999–2000 Arctic vortex: Simulations with the three-dimensional Chemical Lagrangian Model of the Stratosphere (CLaMS), Journal of Geophysical Research: Atmospheres, 109, 2004.

Konopka, P., Günther, G., Müller, R., Dos Santos, F., Schiller, C., Ravegnani, F., Ulanovsky, A., Schlager, H., Volk, C., Viciani, S., et al.: Contribution of mixing to upward transport across the tropical tropopause layer (TTL), 2007.

Konopka, P., Tao, M., Ploeger, F., Diallo, M., and Riese, M.: Tropospheric mixing and parametrization of unresolved convective updrafts as implemented in the Chemical Lagrangian Model of the Stratosphere (CLaMS v2. 0), Geoscientific Model Development, 12, 2441–2462, 2019.

Krämer, M., Schiller, C., Afchine, A., Bauer, R., Gensch, I., Mangold, A., Schlicht, S., Spelten, N., Sitnikov, N., Borrmann, S., et al.: Ice supersaturations and cirrus cloud crystal numbers, Atmospheric Chemistry and Physics, 9, 3505–3522, 2009.

Krämer, M., Rolf, C., Spelten, N., Afchine, A., Fahey, D., Jensen, E., Khaykin, S., Kuhn, T., Lawson, P., Lykov, A., Pan, L. L., Riese, M., Rollins, A., Stroh, F., Thornberry, T., Wolf, V., Woods, S., Spichtinger, P., Quaas, J., and Sourdeval, O.: A Microphysics Guide to Cirrus – Part II: Climatologies of Clouds and Humidity from Observations, Atmospheric Chemistry and Physics Discussions, 2020, 1–63, https://doi.org/10.5194/acp-2020-40, https://www.atmos-chem-phys-discuss.net/acp-2020-40/, 2020.

Lambert, A., Read, W., and Livesey, N.: MLS/Aura Level 2 Water Vapor (H2O) Mixing Ratio V004, Greenbelt, MD, USA, Goddard Earth Sciences Data and Information Services Center (GES DISC), 2015.

Livesey, N., Read, W., Wagner, P., Froidevaux, L., Lambert, A., Manney, G., Millán Valle, L., Pumphrey, H., Santee, M., Schwartz, M., et al.: Version 4.2 x Level 2 data quality and description document, Jet Propul, Tech. rep., Lab., Tech. Rep. JPL D-33509 Rev. D, Pasadena, CA, USA (Available from http . . . , 2018.

Marti, J. and Mauersberger, K.: A survey and new measurements of ice vapor pressure at temperatures between 170 and 250K, Geophysical Research Letters, 20, 363–366, 1993.

McKenna, D. S., Grooß, J.-U., Günther, G., Konopka, P., Müller, R., Carver, G., and Sasano, Y.: A new Chemical Lagrangian Model of the Stratosphere (CLaMS) 2. Formulation of chemistry scheme and initialization, Journal of Geophysical Research: Atmospheres, 107, ACH–4, 2002a.

McKenna, D. S., Konopka, P., Grooß, J.-U., Günther, G., Müller, R., Spang, R., Offermann, D., and Orsolini, Y.: A new Chemical Lagrangian Model of the Stratosphere (CLaMS) 1. Formulation of advection and mixing, Journal of Geophysical Research: Atmospheres, 107, ACH–15, 2002b.

Mote, P. W., Rosenlof, K. H., McIntyre, M. E., Carr, E. S., Gille, J. C., Holton, J. R., Kinnersley, J. S., Pumphrey, H. C., Russell III, J. M., and Waters, J. W.: An atmospheric tape recorder: The imprint of tropical tropopause temperatures on stratospheric water vapor, Journal of Geophysical Research: Atmospheres, 101, 3989–4006, 1996.

Murphy, D. M. and Koop, T.: Review of the vapour pressures of ice and supercooled water for atmospheric applications, Quarterly Journal of the Royal Meteorological Society: A journal of the atmospheric sciences, applied meteorology and physical oceanography, 131, 1539–1565, 2005.

https://doi.org/10.5194/acp-2020-1010
Preprint. Discussion started: 27 October 2020

Nützel, M., Podglajen, A., Garny, H., and Ploeger, F.: Quantification of water vapour transport from the Asian monsoon to the stratosphere, Atmospheric Chemistry and Physics, 19, 8947–8966, 2019.

Pan, L., Konopka, P., and Browell, E.: Observations and model simulations of mixing near the extratropical tropopause, Journal of Geophysical Research: Atmospheres, 111, 2006.

Park, M., Randel, W. J., Gettelman, A., Massie, S. T., and Jiang, J. H.: Transport above the Asian summer monsoon anticyclone inferred from Aura Microwave Limb Sounder tracers, Journal of Geophysical Research: Atmospheres, 112, 2007.

Ploeger, F., Konopka, P., Günther, G., Grooß, J.-U., and Müller, R.: Impact of the vertical velocity scheme on modeling transport in the tropical tropopause layer, Journal of Geophysical Research: Atmospheres, 115, 2010.

Ploeger, F., Günther, G., Konopka, P., Fueglistaler, S., Müller, R., Hoppe, C., Kunz, A., Spang, R., Grooß, J.-U., and Riese, M.: Horizontal water vapor transport in the lower stratosphere from subtropics to high latitudes during boreal summer, Journal of Geophysical Research: Atmospheres, 118, 8111–8127, 2013.

Ploeger, F., Gottschling, C., Griessbach, S., Grooss, J.-U., Guenther, G., Konopka, P., Müller, R., Riese, M., Stroh, F., Tao, M., et al.: A potential vorticity-based determination of the transport barrier in the Asian summer monsoon anticyclone, Atmospheric chemistry and physics, 15, 13 145, 2015.

Ploeger, F., Konopka, P., Walker, K., and Riese, M.: Quantifying pollution transport from the Asian monsoon anticyclone into the lower stratosphere, Atmospheric Chemistry and Physics, 17, 7055, 2017.

Podglajen, A., Bui, T. P., Dean-Day, J. M., Pfister, L., Jensen, E. J., Alexander, M. J., Hertzog, A., Kärcher, B., Plougonven, R., and Randel, W. J.: Small-scale wind fluctuations in the tropical tropopause layer from aircraft measurements: Occurrence, nature, and impact on vertical mixing, Journal of the Atmospheric Sciences, 74, 3847–3869, 2017.

Pommrich, R., Müller, R., Grooss, J.-U., Konopka, P., Ploeger, F., Vogel, B., Tao, M., Hoppe, C., Günther, G., Spelten, N., et al.: Tropical troposphere to stratosphere transport of carbon monoxide and long-lived trace species in the Chemical Lagrangian Model of the Stratosphere (CLaMS), Geoscientific model development, pp. 2895–2916, 2014.

Poshyvailo, L., Müller, R., Konopka, P., Günther, G., Riese, M., Podglajen, A., and Ploeger, F.: Sensitivities of modelled water vapour in the lower stratosphere: temperature uncertainty, effects of horizontal transport and small-scale mixing, Atmospheric Chemistry and Physics, 18, 8505–8527, 2018.

Randel, W. J. and Park, M.: Deep convective influence on the Asian summer monsoon anticyclone and associated tracer variability observed with Atmospheric Infrared Sounder (AIRS), Journal of Geophysical Research: Atmospheres, 111, 2006.

Randel, W. J., Park, M., Emmons, L., Kinnison, D., Bernath, P., Walker, K. A., Boone, C., and Pumphrey, H.: Asian monsoon transport of pollution to the stratosphere, Science, 328, 611–613, 2010.

Randel, W. J., Zhang, K., and Fu, R.: What controls stratospheric water vapor in the NH summer monsoon regions?, Journal of Geophysical Research: Atmospheres, 120, 7988–8001, 2015.

Riese, M., Ploeger, F., Rap, A., Vogel, B., Konopka, P., Dameris, M., and Forster, P.: Impact of uncertainties in atmospheric mixing on simulated UTLS composition and related radiative effects, Journal of Geophysical Research: Atmospheres, 117, 2012.

Santee, M., Manney, G., Livesey, N., Schwartz, M., Neu, J., and Read, W.: A comprehensive overview of the climatological composition of the Asian summer monsoon anticyclone based on 10 years of Aura Microwave Limb Sounder measurements, Journal of Geophysical Research: Atmospheres, 122, 5491–5514, 2017.

Schoeberl, M. and Dessler, A.: Dehydration of the stratosphere, 1foldr Import 2019-10-08 Batch 2, 2011.

https://doi.org/10.5194/acp-2020-1010
Preprint. Discussion started: 27 October 2020

Atmospheric Chemistry and Physics Discussions

Schoeberl, M., Dessler, A., and Wang, T.: Simulation of stratospheric water vapor and trends using three reanalyses, 1foldr Import 2019-10-08 Batch 13, 2012.

Schoeberl, M., Dessler, A., and Wang, T.: Modeling upper tropospheric and lower stratospheric water vapor anomalies, 1foldr Import 2019-10-08 Batch 6, 2013.

Schoeberl, M., Jensen, E., Pfister, L., Ueyama, R., Wang, T., Selkirk, H., Avery, M., Thornberry, T., and Dessler, A.: Water vapor, clouds, and saturation in the tropical tropopause layer, Journal of Geophysical Research: Atmospheres, 124, 3984–4003, 2019.

Schoeberl, M. R., Dessler, A. E., Wang, T., Avery, M. A., and Jensen, E. J.: Cloud formation, convection, and stratospheric dehydration, Earth and Space Science, 1, 1–17, 2014.

Schoeberl, M. R., Jensen, E. J., Pfister, L., Ueyama, R., Avery, M., and Dessler, A. E.: Convective hydration of the upper troposphere and lower stratosphere, Journal of Geophysical Research: Atmospheres, 123, 4583–4593, 2018.

Solomon, S., Rosenlof, K. H., Portmann, R. W., Daniel, J. S., Davis, S. M., Sanford, T. J., and Plattner, G.-K.: Contributions of stratospheric water vapor to decadal changes in the rate of global warming, Science, 327, 1219–1223, 2010.

Tao, M., Konopka, P., Ploeger, F., Yan, X., Wright, J. S., Diallo, M., Fueglistaler, S., and Riese, M.: Multitimescale variations in modeled stratospheric water vapor derived from three modern reanalysis products, Atmospheric Chemistry and Physics, 19, 6509–6534, https://doi.org/10.5194/acp-19-6509-2019, https://www.atmos-chem-phys.net/19/6509/2019/, 2019.

Ueyama, R., Jensen, E. J., and Pfister, L.: Convective influence on the humidity and clouds in the tropical tropopause layer during boreal summer, Journal of Geophysical Research: Atmospheres, 123, 7576–7593, 2018.

Von Hobe, M., Grooß, J.-U., Günther, G., Konopka, P., Gensch, I., Krämer, M., Spelten, N., Afchine, A., Schiller, C., Ulanovsky, A., et al.: Evidence for heterogeneous chlorine activation in the tropical UTLS, Atmospheric Chemistry and Physics, 11, 241, 2011.

Wang, T. and Dessler, A. E.: Analysis of cirrus in the tropical tropopause layer from CALIPSO and MLS data: A water perspective, Journal of Geophysical Research: Atmospheres, 117, 2012.

Wang, X., Dessler, A. E., Schoeberl, M. R., Yu, W., and Wang, T.: Impact of convectively lofted ice on the seasonal cycle of water vapor in the tropical tropopause layer, Atmospheric Chemistry and Physics, 19, 14 621–14 636, 2019.

Waters, J. W., Froidevaux, L., Harwood, R. S., Jarnot, R. F., Pickett, H. M., Read, W. G., Siegel, P. H., Cofield, R. E., Filipiak, M. J., Flower, D. A., et al.: The earth observing system microwave limb sounder (EOS MLS) on the Aura satellite, IEEE Transactions on Geoscience and Remote Sensing, 44, 1075–1092, 2006.

Yan, X., Konopka, P., Ploeger, F., Podglajen, A., Wright, J. S., Müller, R., and Riese, M.: The efficiency of transport into the stratosphere via the Asian and North American summer monsoon circulations, Atmospheric Chemistry and Physics, 19, 15 629–15 649, 2019.

Ye, H., Dessler, A. E., and Yu, W.: Effects of convective ice evaporation on interannual variability of tropical tropopause layer water vapor, Atmospheric Chemistry and Physics, 18, 4425–4437, 2018.

Zhang, K., Fu, R., Wang, T., and Liu, Y.: Impact of geographic variations of convective and dehydration center on stratospheric water vapor over the Asian monsoon region, 1foldr Import 2019-10-08 Batch 8, 2016.

https://doi.org/10.5194/acp-2020-1010
Preprint. Discussion started: 27 October 2020

Atmospheric Chemistry and Physics Discussions

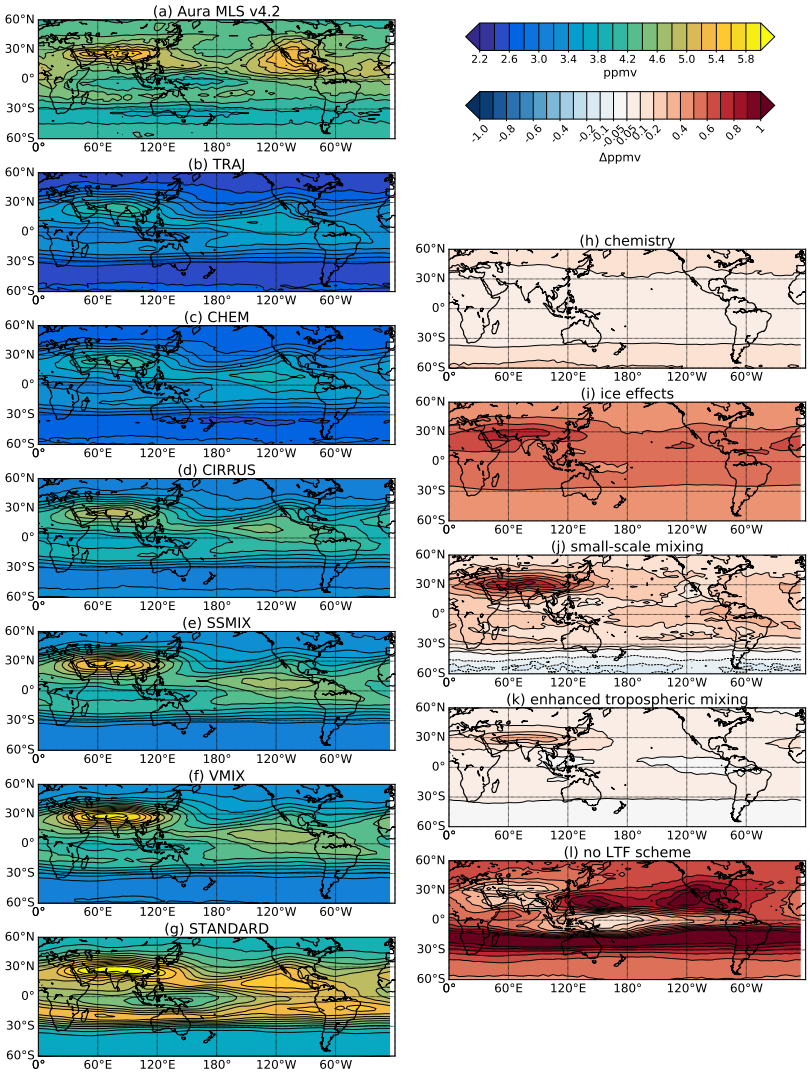

Figure 1. (Left column) Climatology of water vapour distribution at 100 hPa during boreal summer (June-July-August) for the period 2007–2016 from **(a)** Aura MLS v4.2 observations, **(b)** TRAJ, **(c)** CHEM, **(d)** CIRRUS, **(e)** VMIX, **(f)** SSMIX experiments and **g)** STANDARD simulation. (Right column) Isolated effect of each **h)** chemistry, **i)** cirrus, **j)** small-scale mixing, **k)** enhanced tropospheric mixing and **l)** no LTF scheme. In the case of TRAJ, the water vapour simulated is the lowest mixing ratio encountered by the air parcels in its trajectory following the empirical mixing ratio equation from Murphy and Koop (2005). For the rest of experiments water vapour has been simulated applying each parameterization along the trajectory of the air parcel. As each experiment is configured including a new parameterization into the previous model version, the effect of each parameterization can be isolated computing the differences between consecutive experiments. Air parcels have been binned to 5°-longitude x 2°-latitude grid.

https://doi.org/10.5194/acp-2020-1010
Preprint. Discussion started: 27 October 2020

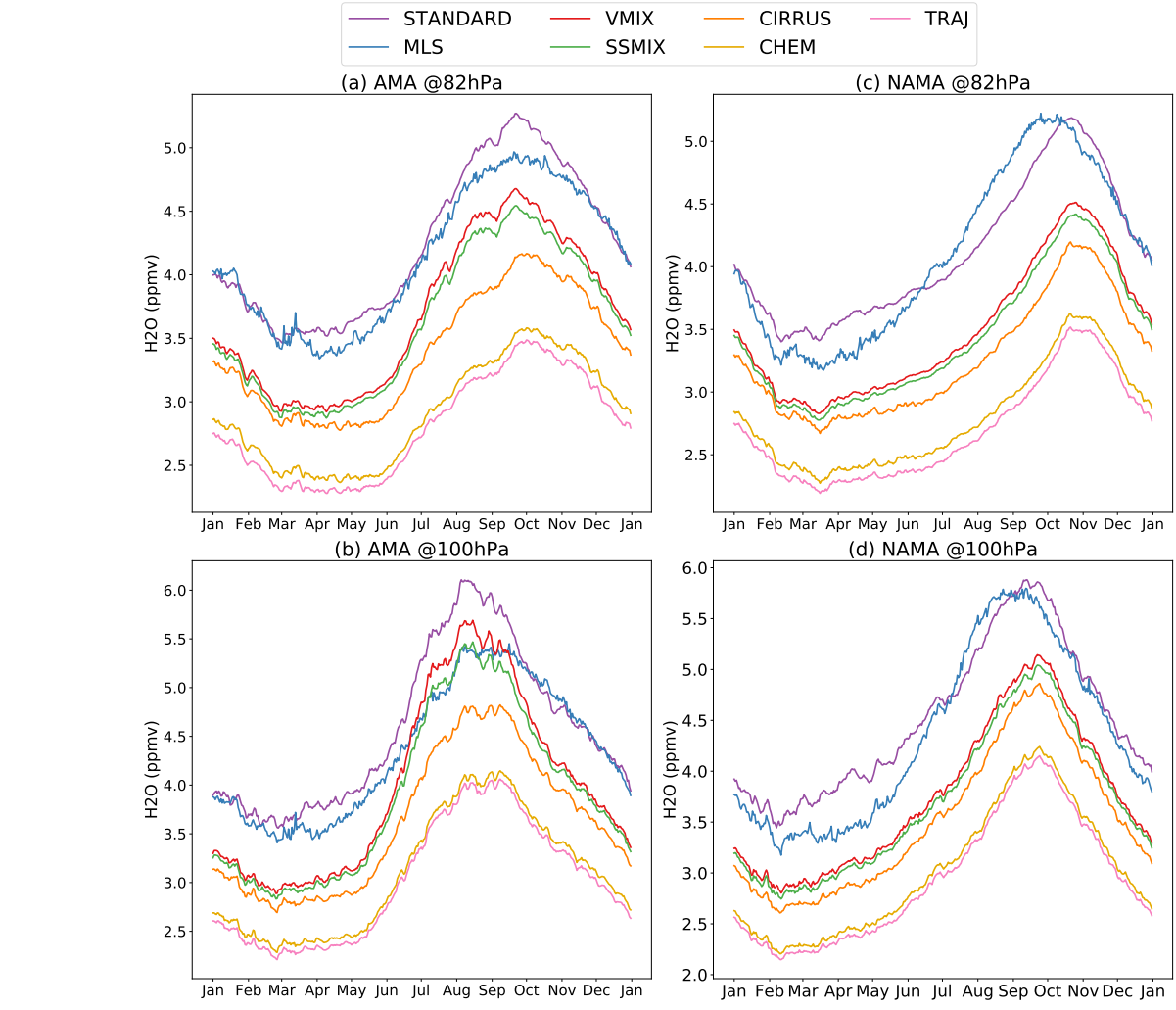

Figure 2. Annual cycle of daily water vapour at (top) 80 hPa and (bottom) 100 hPa averaged over **(a, b)** the Asian Monsoon Anticyclone, AMA (20°N–40°N, 40°E–140°E) and **(c, d)** the North American Monsoon Anticyclone, NAMA (10°N–30°N, 220°E–300°E) for the period 2007–2016. The regions in which averages are computed correspond to the maxima of water vapour found in the boreal summer climatology of the water vapour observed by Aura MLS v4.2.

https://doi.org/10.5194/acp-2020-1010
Preprint. Discussion started: 27 October 2020

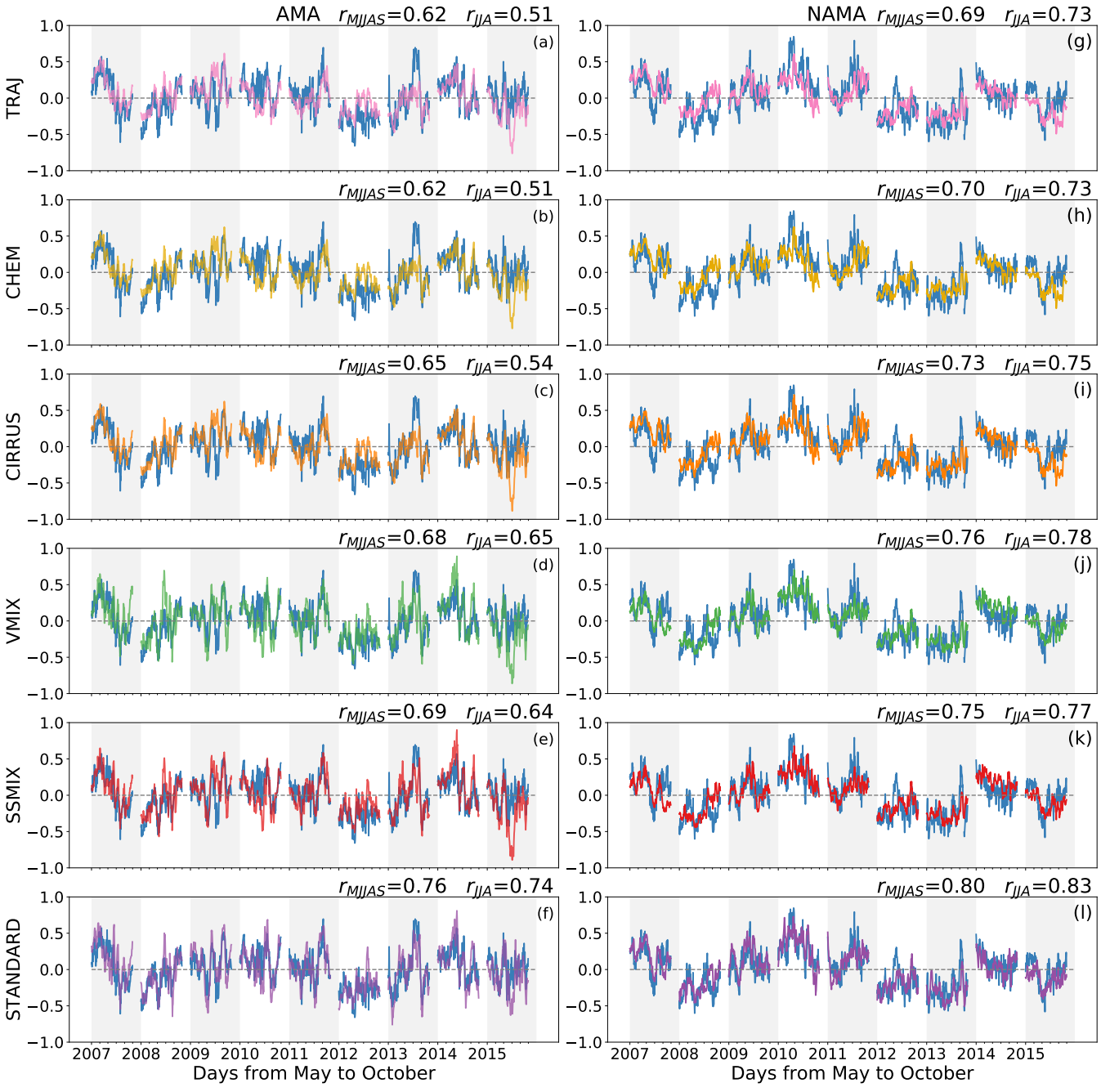

Figure 3. Boreal summer deseasonalized anomalies of water vapour in (left column) the Asian Monsoon Anticyclone, AMA, and (right column) the North American Monsoon Anticyclone, NAMA, for (top-bottom) TRAJ, CHEM, CIRRUS, VMIX, SSMIX, STANDARD in comparison with MLS (blue line). Correlation values between each experiment and MLS are calculated from May to Sep (r_{MJJAS}) and from June to Aug (r_{JJA}).

https://doi.org/10.5194/acp-2020-1010
Preprint. Discussion started: 27 October 2020

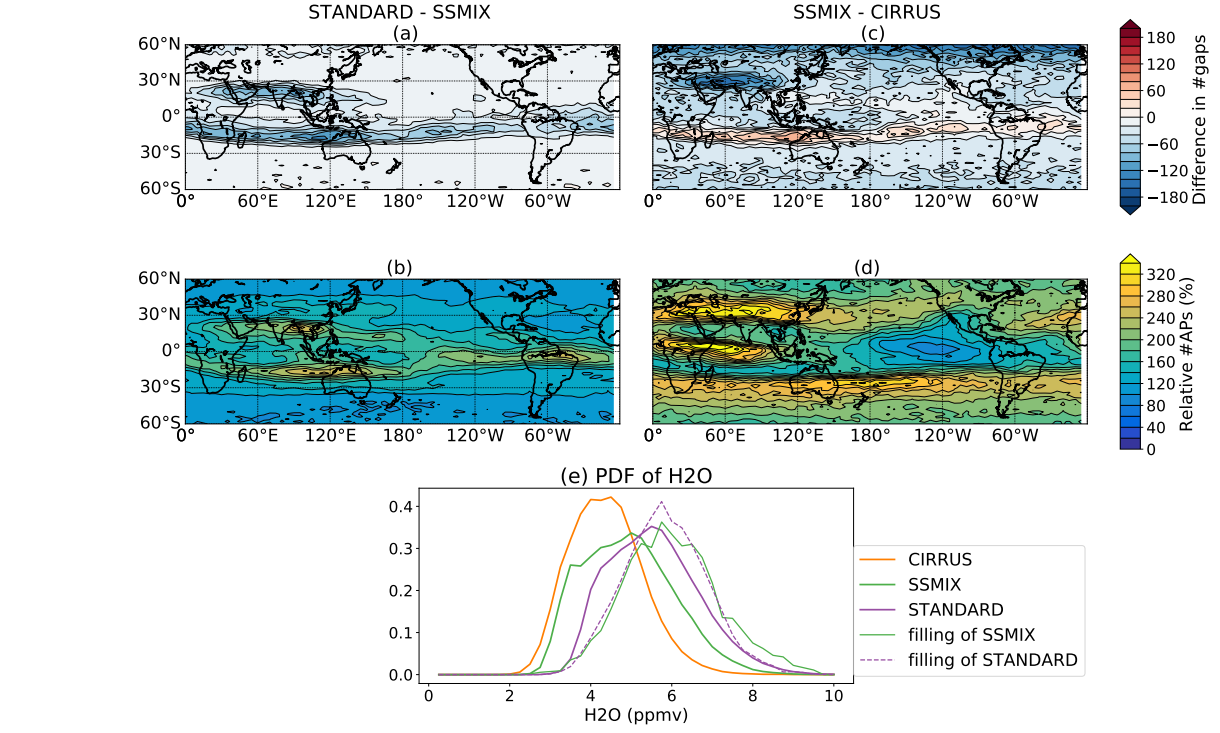

Figure 4. (Top row) Differences in the total number of gaps found during JJA between 2007-2016 of **(a)** STANDARD against SSMIX and **(c)** SSMIX against CIRRUS. (Middle) Distribution of the relative number of air parcels simulated in **(b)** STANDARD with respect to SSMIX and in **(d)** SSMIX with respect to CIRRUS during JJA for 2007–2016. (Bottom) **(e)** PDF of the water vapour of bins (solid line) and gaps (dashed line) during JJA (2007–2016) over the Asian Monsoon region (20°–40°N, 40°–140°E) for CIRRUS, SSMIX and STANDARD. The water vapour content of the gaps (empty bins) is calculated from the respective reference experiment without gaps, hence for the gaps of SSMIX from the STANDARD water vapour distribution (purple dashed line) and for the gaps of CIRRUS from the SSMIX water vapour (green dashed line). The water vapour content of a bin in the map is the mean water vapour content of the air parcels in it. The bin size is 5°-longitude x 2°-latitude.

https://doi.org/10.5194/acp-2020-1010
Preprint. Discussion started: 27 October 2020

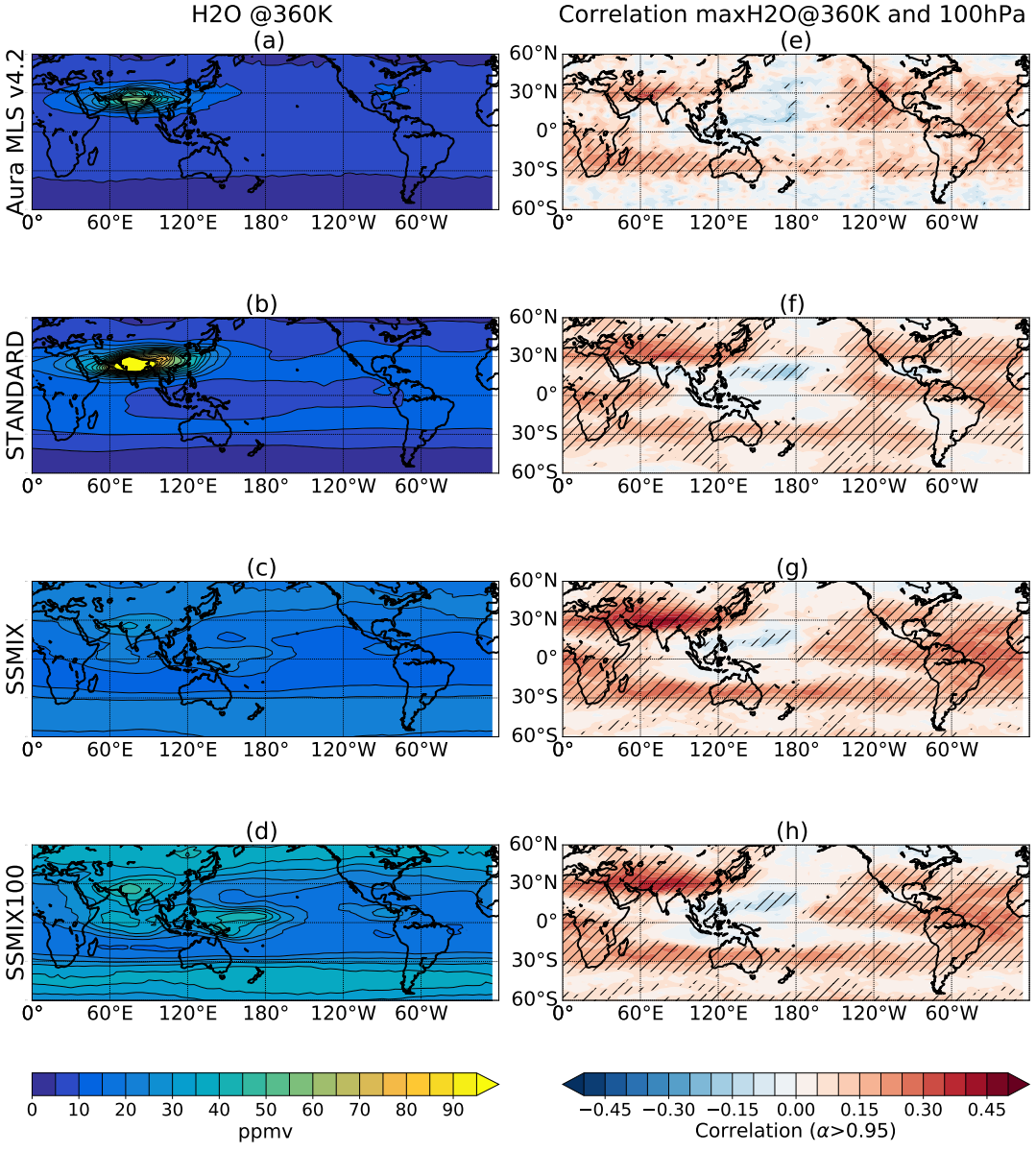

Figure 5. (Left column) Climatology of water vapour at 360 K from **(a)** Aura MLS v4.2 observations, **(b)** STANDARD, **(c)** SSMIX and **(d)** SSMIX initialized with 100 ppmv. (right column) Correlation between the water vapour timeseries averaged in 60°E–100°E, 20°N–30°N at 360 K and the timeseries of water vapour at 100 hPa at each grid point during boreal summer for **(e)** Aura MLS v4.2 **(f)** STANDARD, **(g)** SSMIX and **(h)** SSMIX initialized with 100 ppmv.

https://doi.org/10.5194/acp-2020-1010
Preprint. Discussion started: 27 October 2020

Atmospheric Chemistry and Physics Discussions

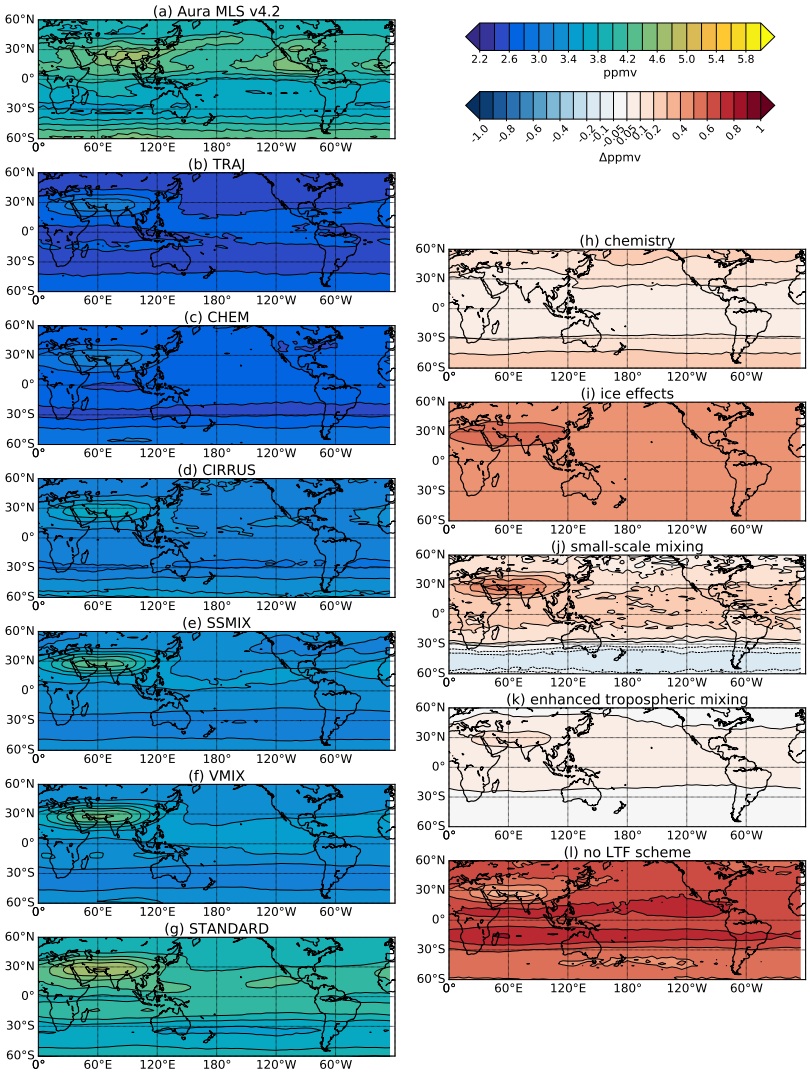

Figure A1. (Left column) Climatology of water vapour distribution at 80 hPa during boreal summer (JJA) for the period 2007-2016 from **(a)** Aura MLS v4.2 observations, **(b)** TRAJ, **(c)**CHEM, **(d)**CIRRUS, **(e)**VMIX, **(f)**SSMIX experiments and **(g)**STANDARD simulation. (Right column) Isolated effect of each **(h)**chemistry, **(i)** cirrus, **(j)** small-scale mixing, **(k)** enhanced tropospheric mixing and **(l)** no LTF scheme. In the case of TRAJ, the water vapour simulated is the lowest mixing ratio encountered by the air parcels in its trajectory following the empirical mixing ratio equation from Murphy and Koop (2005). For the rest of experiments water vapour has been simulated applying each parameterization along the trajectory of the air parcel. As each experiment is configured including a new parameterization into the previous model version, the effect of each parameterization can be isolated computing the differences between consecutive experiments. Air parcels have been binned to 5°-longitude x 2°-latitude grid.

https://doi.org/10.5194/acp-2020-1010
Preprint. Discussion started: 27 October 2020

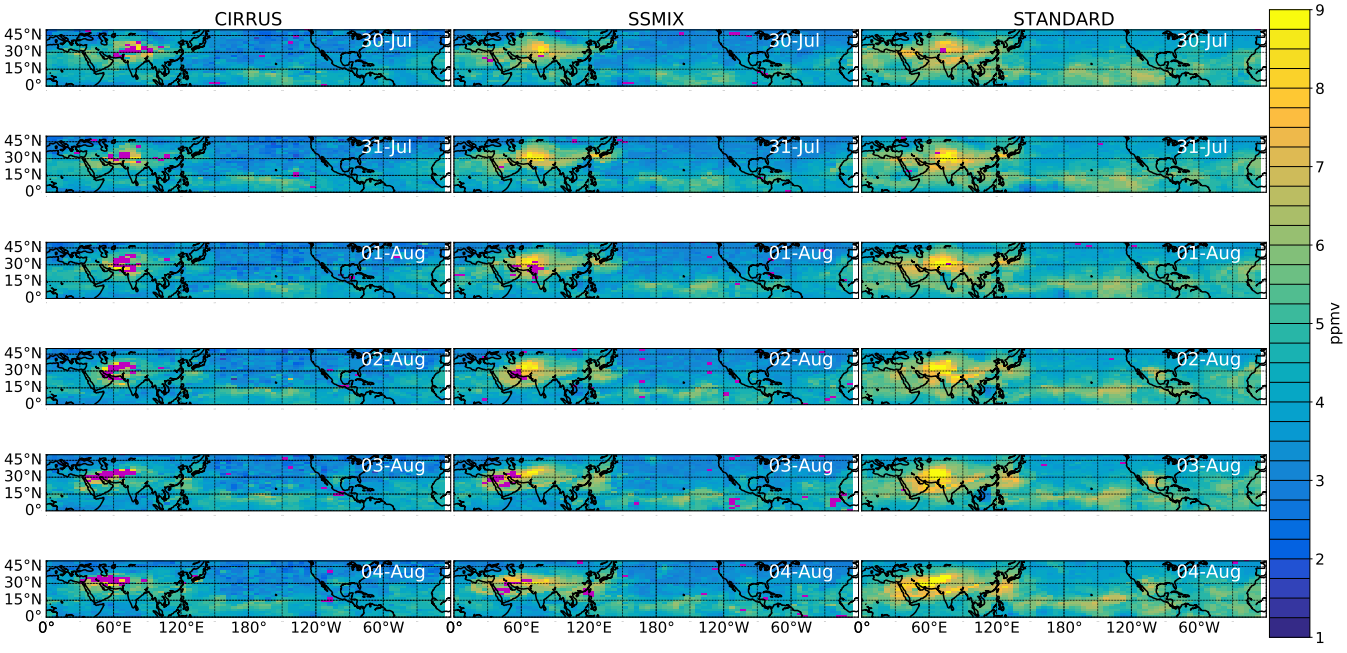

Figure A2. Daily distributions of water vapour at 100 hPa from (top to bottom) 30 of July to 4 August 2013 of (from left to right) CIRRUS, SSMIX and STANDARD. Empty bins or "gaps" are represented by magenta bins.

https://doi.org/10.5194/acp-2020-1010
Preprint. Discussion started: 27 October 2020

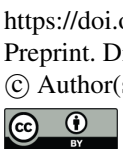

Atmospheric Chemistry and Physics Discussions

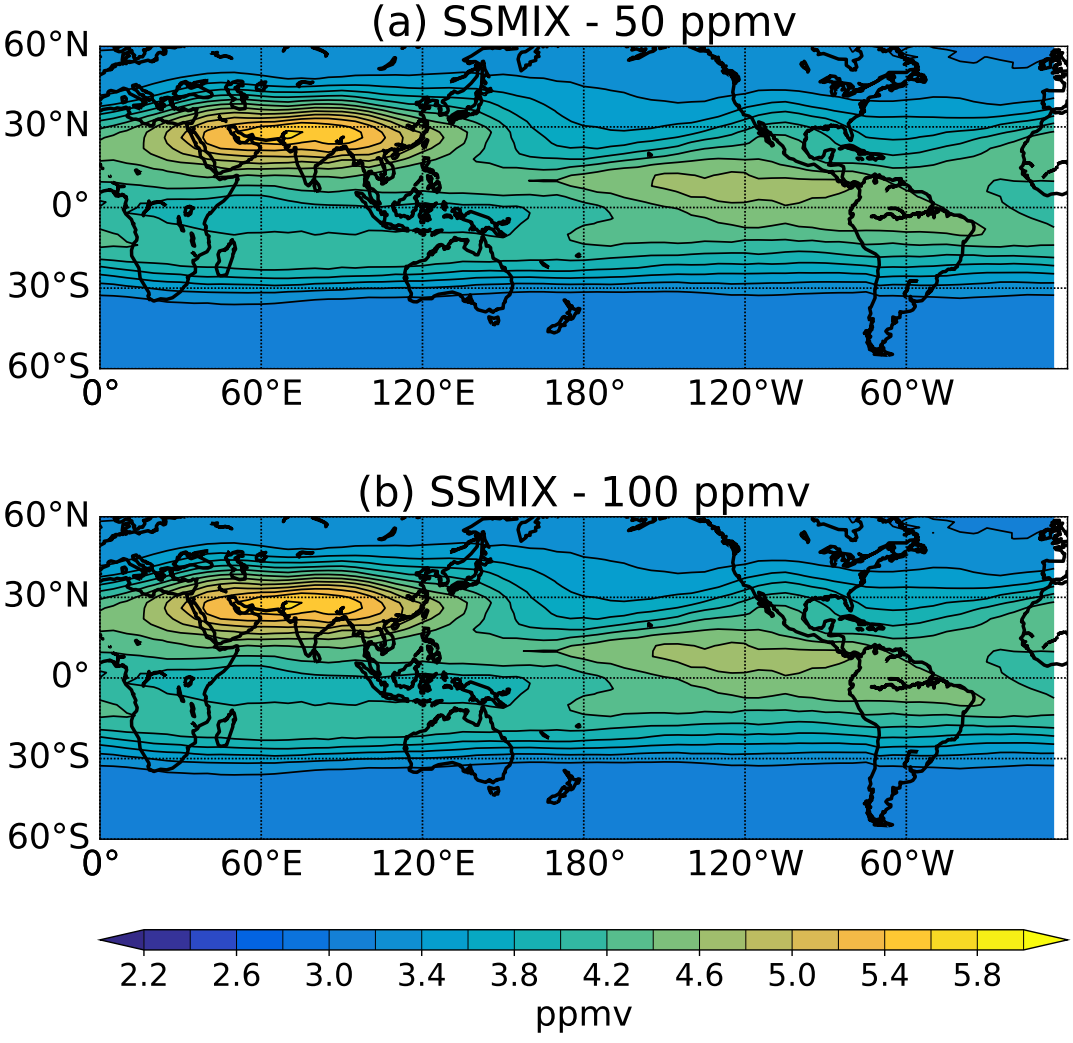

Figure A3. Distribution of water vapour at 100 hPa of SSMIX initialized with **(a)** 50 ppmv and **(b)** 100 ppmv during boreal summer for 2007–2016.

https://doi.org/10.5194/acp-2020-1010
Preprint. Discussion started: 27 October 2020

Atmospheric Chemistry and Physics Discussions

Table 1. Description of experiments done with CLaMS

Experiment	Configuration	Timestep	H2O at 360K	#Air parcels	Further details
TRAJ	LTF	6h	None	∼412000	Pure advective trajectories using ERAinterim horizontal wind fields and diabatic heating rate.
CHEM	TRAJ + chemistry module	6h	50	∼412000	Only methane oxidation
CIRRUS	CHEM + cirrus scheme	6h	50	∼412000	characteristic length set to ∼300m
SSMIX	CIRRUS + small-scale mixing	24h	50	∼1026000	After mixing, cirrus scheme is applied again
VMIX	SSMIX + tropospheric mixing	24h	50	∼1026000	After mixing, cirrus scheme is applied again
STANDARD	SSMIX + ST-Filling	24h	ERAInterim	∼2000000	After mixing, cirrus scheme is applied again. Full chemistry (see McKenna et al. (2002a)) No LTF set up Water vapour fields from ERAInterim in troposphere below 500 hPa.

Timestep specifies the frequency of the output in each experiment.

#Air parcels is the mean number of air parcels per day after 2-year of spin-up time

LTF *(Lagrangian Trajectory Filling Set Up)*: based in the domain-filling technique developed by Schoeberl and Dessler (2011)

ERAinterim reanalysis from European Centre for Medium Range Weather Forecasts